

# The interplay of the $3d^9$ and $3d^{10}\underline{L}$ electronic configurations in the copper $K$ -edge XANES spectra of Cu(II) compounds

Jesús Chaboy,<sup>a\*</sup> Adela Muñoz-Páez<sup>b</sup> and Enrique Sánchez Marcos<sup>c</sup>

<sup>a</sup>Instituto de Ciencia de Materiales de Aragón, CSIC - Universidad de Zaragoza, 50009 Zaragoza, Spain, <sup>b</sup>Departamento de Química Inorgánica - ICMSE, CSIC - Universidad de Sevilla, 41012 Sevilla, Spain, and <sup>c</sup>Departamento de Química Física, Universidad de Sevilla, 41012 Sevilla, Spain. E-mail: jchaboy@unizar.es

A theoretical analysis of the X-ray absorption near-edge structure spectra at the Cu  $K$ -edge in several divalent copper [Cu(II)] compounds showing a distorted nearest-neighborhood around copper is presented. The experimental spectra of CuO and  $\text{KCuF}_3$  have been compared with computations performed in the framework of the multiple-scattering theory. The results show that *ab initio* single-channel multiple-scattering calculations are not able to reproduce the experimental spectra. On the contrary, the experimental spectra can be accounted for by using two excitation channels and the sudden limit of the multichannel multiple-scattering theory. The comparison between experimental data and computations indicates that both  $3d^9$  and  $3d^{10}\underline{L}$  electronic configurations are needed to account for the absorption process in these systems, suggesting that this is the general case for the  $K$ -edge XANES of divalent copper compounds.

**Keywords:** X-ray absorption spectroscopy; XANES; multiple scattering.

## 1. Introduction

X-ray absorption spectroscopy (XAS) is nowadays one of the most widespread tools used for local structure determinations (Sayers & Bunker, 1988, and references therein; Iwasawa, 1996). Reliable structural parameters such as interatomic distances, coordination numbers *etc.* are commonly derived from the analysis of the extended X-ray absorption fine-structure (EXAFS) region of the spectrum. The accuracy of these structural determinations has been improved by the development of powerful computer codes (Ankudinov *et al.*, 1998; Joly, 2001; Natoli & Benfatto, 1986).

The study of the near-edge region of the X-ray absorption spectrum (XANES) is now attracting much attention because of its sensitivity to the bonding geometry. Despite the wealth of electronic and structural information of XANES, its usefulness as a structural tool is lower than EXAFS because the computation of XANES and its analysis are not as straightforward as for the EXAFS region. The search for an accurate description of the XANES spectra motivated new studies, from both experimental and theoretical standpoints. Most of these studies have focused on the  $3d$  transition metal  $K$ -edge XANES spectra in simple systems (Briois *et al.*, 1995; Benfatto *et al.*, 1997; Merklings *et al.*, 2001, 2002; D'Angelo *et al.*, 2002). Theoretical calculations have provided good agreement with the experimental spectra for the divalent  $\text{Fe}^{2+}$ ,

$\text{Co}^{2+}$  and  $\text{Ni}^{2+}$  ions in aqueous solutions (Benfatto *et al.*, 1997). Surprisingly, calculations fail to reproduce the experimental spectra of divalent copper (Briois *et al.*, 1995). The latter results cast a shadow over the possibility of extending the range of applicability of XANES analysis to complex Cu systems such as living organisms (Ascone *et al.*, 2003).

In recent work (Chaboy *et al.*, 2005), we have reported a systematic theoretical study of the Cu  $K$ -edge XANES spectra in several divalent copper compounds showing a square-planar Cu–N arrangement of increasing complexity around the metal atom. The main finding of this work is the need to include both  $3d^9$  and  $3d^{10}\underline{L}$  final-state electronic configurations in the presence of the core hole (where  $\underline{L}$  denotes a  $2p$  hole in N from the ligand) in order to reproduce the experimental spectra. The total cross section is obtained as the sum of two absorption channels with a relative weight of 68% ( $3d^{10}\underline{L}$ ) and 32% ( $3d^9$ ). A similar scheme applied to the study of the Cu  $K$ -edge XANES of  $\text{NdCuO}_4$  (Wu *et al.*, 1996) and of the cupric cation  $\text{Cu}^{2+}$  in aqueous solution (Chaboy *et al.*, 2006) also yields a relative weight of  $\sim 0.7$  and  $\sim 0.3$  for the two absorption channels.

In order to verify the generality of the above results, *i.e.* to test whether the two absorption channels scheme is characteristic of divalent copper, we have extended our previous research to Cu(II) systems with other ligands and environments. In this way we have performed a systematic theoretical

study of the Cu *K*-edge XANES spectra in CuO and KCuF<sub>3</sub>. The interpretation of the Cu *K*-edge XANES spectrum in CuO is linked to renewed interest in the basic physical properties of copper oxides after the discovery of high-*T<sub>c</sub>* superconductors. In particular, to what extent can CuO be described within a one-electron formalism, as the importance of strong electron correlations in CuO was stressed in many studies, is still an open question (Sipr, 1992; Bocharov *et al.*, 2001). On the other hand, the pseudocubic perovskite KCuF<sub>3</sub> has attracted significant interest in recent years regarding the problem of orbital ordering and the study of the interactions between orbital, magnetic and structural ordering in strongly correlated 3*d* transition metal compounds (Paolasini *et al.*, 2002; Takahashi *et al.*, 2003; Bingelli & Altarelli, 2004).

The results of the Cu *K*-edge XANES calculations are discussed by showing the improvements obtained by using self-consistent field (SCF) methods to describe the final state of the photoabsorption process. Moreover, the relative weighting of the different electronic configurations involved is also discussed. Our results point out that the need to include a multichannel scheme (Natoli *et al.*, 1990) prior to account for the Cu *K*-edge XANES spectra is not a particular property of Cu–N compounds. On the contrary, they suggest it is the general case for the *K*-edge XANES of divalent copper [Cu(II)] systems.

## 2. Experimental and computational methods

X-ray absorption experiments at the Cu *K*-edge of CuO were performed at beamline BM29 of the ESRF. XANES spectra were recorded in transmission mode using a Si(311) double-crystal monochromator. A detailed description of the experimental XAS set-up can be found by Carrera *et al.* (2004). The raw Cu *K*-edge XANES spectrum of KCuF<sub>3</sub> has been adapted from Nadai *et al.* (1997). In both cases the origin of the energy scale,  $E_0$ , was defined to be at the inflection point of the absorption edge and the XANES spectra were normalized, after background subtraction, at high energy ( $\sim 100$  eV above the edge) to eliminate thickness dependence.

The computation of the XANES spectra was carried out using the multiple-scattering code *CONTINUUM*, based on the one-electron full-multiple-scattering theory (Benfatto *et al.*, 1986). A complete discussion of the procedure can be found in Natoli *et al.* (2003) and Chaboy *et al.* (2005). The calculated theoretical spectra have been further convoluted with a Lorentzian shape function to account for the core-hole lifetime ( $\Gamma = 1.5$  eV) (Krause & Oliver, 1979) and the experimental resolution ( $\Gamma = 1$  eV).

## 3. Results and discussion

### 3.1. CuO

The local structure of Cu in CuO consists of four O atoms in a quasi-planar structure, with interatomic Cu–O distances  $R_1 = 1.95$  Å and  $R_2 = 1.96$  Å (Sipr, 1992). These four atoms form a distorted pyramid with two apical O atoms at  $R_3 =$

2.78 Å from Cu. *Ab initio* single-channel multiple-scattering computations of the Cu *K*-edge of CuO were performed for different cluster sizes around the photoabsorbing Cu atom and by using different treatments of the exchange-correlation potential (ECP) (Chaboy *et al.*, 2005; Natoli *et al.*, 2003).

Starting from the simplest square-planar Cu–O arrangement, further coordination shells are included to build up a cluster of 51 atoms, *i.e.* covering contributions from atoms located within the first 5 Å around Cu. The addition of further shells does not produce major changes.

The cluster potential was approximated by a set of spherically averaged muffin-tin potentials built by following the standard Mattheis prescription (Mattheis, 1964). The radii of the muffin-tin potentials centered on the atomic sites were determined following Norman's criterion and by imposing a 10% overlapping factor (Norman, 1974). The Coulomb part of each atomic potential was generated using charge densities for neutral atoms obtained from the tabulated atomic wavefunctions of Clementi & Roetti (1974). The final-state potential was built according to the screened  $Z + 1$  approximation (Lee & Beni, 1977) and by adding an appropriate exchange and correlation potential.

Fig. 1 reports a comparison of the experimental CuO spectrum with that of the theoretical computation obtained by using the screened  $Z + 1$  approximation and complex Hedin–Lundqvist ECP for the construction of the final-state potential. The Cu *K*-edge experimental spectrum of CuO shows different absorption features: (i) a step-like peak (A) at the raising edge; (ii) a main absorption line composed of up to three contributions (B  $\simeq 8.6$  eV; C  $\simeq 13.4$  eV; D  $\simeq 17$  eV); (iii) a split (E  $\simeq 27$  eV; F  $\simeq 33$  eV) feature at the high-energy side of the main line; and finally (iv) a deep minimum (G  $\simeq 43$  eV) and a broad positive resonance (H  $\simeq 65$  eV) at higher energies. The single-channel theoretical calculations do not reproduce the experimental spectral shape of CuO, independently of the ECP used for the calculation. The calculation returns the step-like feature A and a single main line whose energy position and width resemble those of the spectral feature B. By contrast both C and D structures, at the main peak, and feature F, in the high-energy region, are not accounted for by the calculation. Moreover, the calculated G and H spectral features fall short of the experimental ones. The comparison is not improved by changing the constant parameter  $\Gamma_C$  used for the convolution of the theoretical spectrum to account for the core-hole lifetime and the experimental resolution.

The disagreement between the theoretical calculations and the experimental spectrum is not due either to structural effects or to a bad choice of the interstitial potential. Indeed, as shown in Fig. 1(b), no significant modification of the narrow single-peak spectral profile is obtained by (i) increasing the size of the cluster (from 51 to 135 atoms) to include contributions from atoms located within the first 7.1 Å around Cu; and (ii) by imposing different (1%, 10% and 20%) overlapping factors of the muffin-tin spheres to modify *ad hoc* their scattering power, and in a second instance to decrease the volume of the interstitial region (Natoli *et al.*, 2003). At this

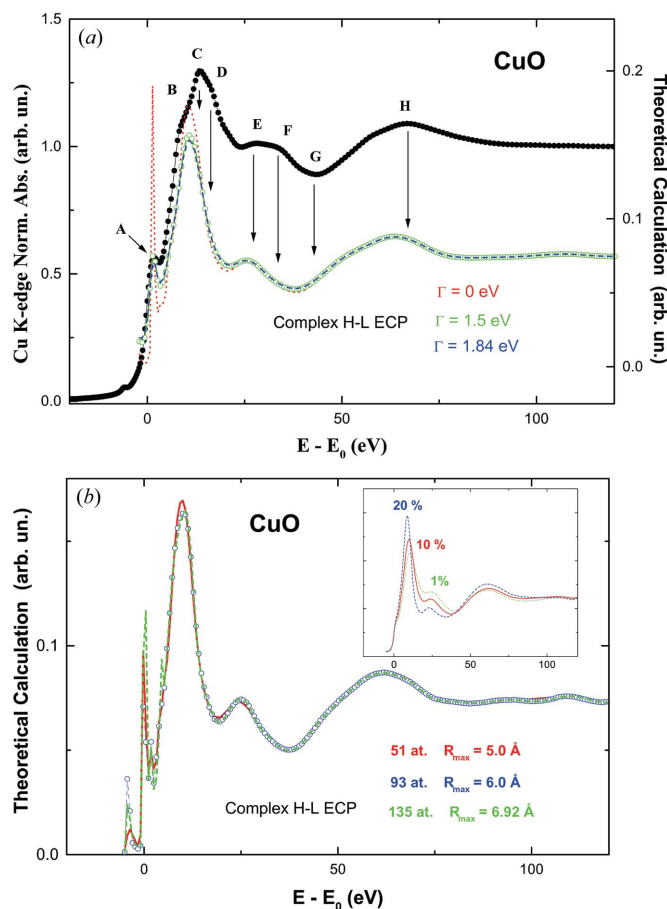


**Figure 1**

(a) Comparison of the experimental XANES spectrum at the Cu *K*-edge in CuO (circles) and the theoretical spectra computed by using a complex Hedin–Lundqvist ECP and different convolution parameter:  $\Gamma_c = 1.5$  eV (green, open circles), 1.84 eV (blue, dashed line) and without convolution (red, dotted line). (b) Comparison of the computed XANES spectra calculated by using a complex Hedin–Lundqvist ECP for different cluster sizes: 51 atoms (red, solid line), 93 atoms (blue, open circles) and 135 atoms (green, dashed line). Spectra are shown without convolution for the sake of clarity. In the inset the computation performed for the 51 atoms cluster by using different overlapping factors (see text for details) is shown: 1% (green, dotted line), 10% (red, solid line) and 20% (blue, dashed line). Colour versions of the figures are available in the online version of the paper.

point it is instructive to compare the width of the main Cu *K*-edge absorption line for the systems under study with that of the tetramminecopper(II) aqueous solution (Chaboy *et al.*, 2005). As shown in Fig. 2, this width is similar in the considered cases, and twice that of the *K*-edge XANES spectra of different divalent transition metals (Fe, Co, Ni) in aqueous solution (Benfatto *et al.*, 1997). This result suggests the need to include two different excitation channels, as in the case of tetramminecopper(II) (Chaboy *et al.*, 2005), to account for the Cu *K*-edge XANES spectra of the selected Cu(II) compounds.

As with the previous results (Chaboy *et al.*, 2005), we have used SCF potentials for the different electronic configurations used in the calculations:  $3d^9$  and  $3d^{10}\underline{L}$ , where  $\underline{L}$  denotes a  $2p$  hole in the ligand oxygen atom. The excited final-state potential was calculated by promoting one of the  $1s$  electrons of Cu to the first free energy level of the right symmetry and

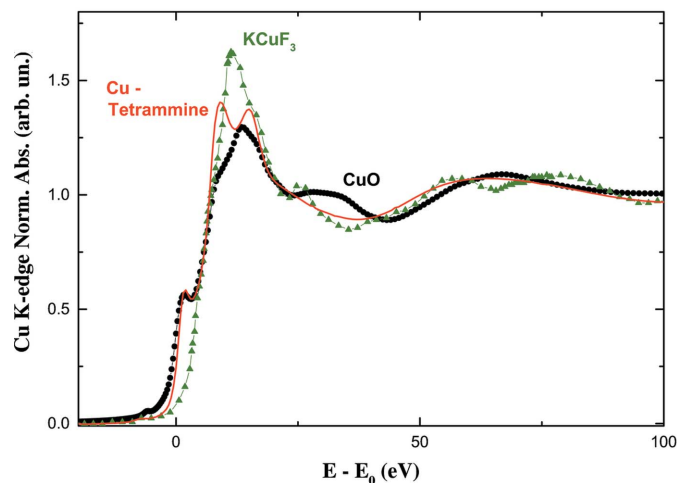


**Figure 2**

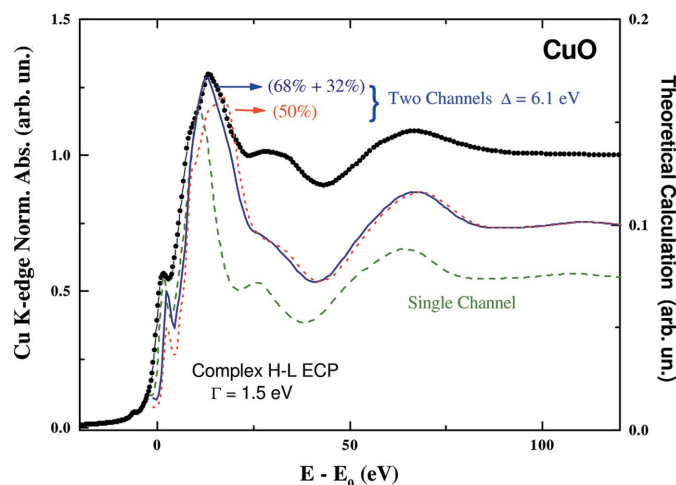
Comparison of the experimental XANES spectrum at the Cu *K*-edge in CuO (circles), aqueous solution of tetramminecopper(II) (solid line) and  $\text{KCuF}_3$  (triangles).

fixing to one the  $1s$  occupancy during the SCF procedure. The energy of the process is then given by the difference between the total energy of the excited final state and the initial ground state. We have (SCF) stabilized a small  $[\text{CuO}_4]^{6-}$  cluster with an outer sphere with a 6+ charge to neutralize the whole cluster. This cluster has been embedded in the larger ones in order to perform the multiple-scattering calculations. Then, the potential of both the absorbing Cu and the four next-neighbor O atoms is SCF, while the potential around the other atoms was built according to Mattheis' prescription. This procedure has been previously shown to be successful on extended systems (Wu *et al.*, 1992; Pedio *et al.*, 1994). Both  $3d^9$  and  $3d^{10}\underline{L}$  configurations give rise to two absorption edges shifted in energy by  $\Delta = 6.1$  eV, close to the values found for other Cu(II) systems (Chaboy *et al.*, 2005, 2006). As shown in Fig. 3, a remarkable agreement is found between the experimental data and the Cu *K*-edge cross section computed as the sum of both  $3d^{10}\underline{L}$  and  $3d^9$  contributions with fixed relative weights of 68% and 32%, respectively (Chaboy *et al.*, 2005). These factors, close to the values reported by Wu *et al.* (1996), were fixed throughout this study.

### 3.2. $\text{KCuF}_3$

The results obtained for CuO suggest that the two absorption channels ( $3d^{10}\underline{L}$  and  $3d^9$ ) scheme is a general characteristic of Cu(II) *K*-edge XANES spectra, the relative weight of both channels being close to the 70:30 ratio. Further confirmation of this result can be obtained by computing the Cu *K*-edge X-ray absorption of Cu(II) in  $\text{KCuF}_3$ .

Research into the  $\text{KCuF}_3$  compound has recently attracted much attention owing to its links with the development of the resonant elastic X-ray scattering (RXS) technique that has been postulated as an incomparable tool for probing orbital ordering (Paolasini *et al.*, 2002). The theoretical interpretation of the RXS spectra is being developed and several questions still remain open regarding the role of the spin polarization

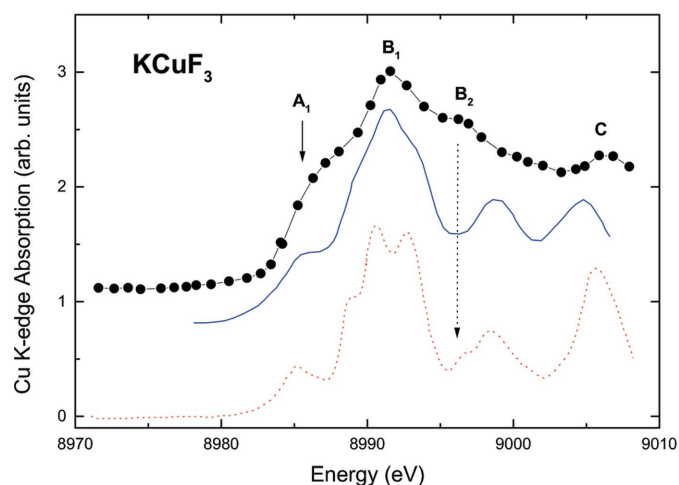

**Figure 3**

Comparison of the experimental XANES spectrum at the Cu *K*-edge in CuO and the theoretical spectrum obtained as the weighted sum of the  $3d^9$  (32%) and  $3d^{10}L$  (68%) contributions (solid line); equal weighting (50%) of both channels (dotted line) and the calculation performed on the single-channel approximation (dashed line). All the calculations have been performed by using the Hedin–Lundqvist ECP and a convolution parameter  $\Gamma_C = 1.84$  eV (see text for details).

versus the orbital polarization in determining the RXS spectra (Takahashi *et al.*, 2003; Bingelli & Altarelli, 2004).

The RXS at the Cu *K*-edge in  $\text{KCuF}_3$  derives from a virtual dipolar excitation to the empty  $4p$  states. The resulting RXS amplitude is thus not directly related to the  $3d$  states that exhibit orbital ordering, but to the anisotropy induced in the surrounding  $4p$  states. This indirect dependence makes the interpretation of the RXS results difficult (Takahashi *et al.*, 2003; Bingelli & Altarelli, 2004). Indeed, recent calculations have shown that the Cu *K*-edge RXS in  $\text{KCuF}_3$  is more sensitive to the Jahn–Teller distortion that accompanies the orbital ordering rather than to the orbital ordering itself (Bingelli & Altarelli, 2004). One of the key points for the computation of the RXS at the Cu *K*-edge is the calculation of the density of states (DOS). The performance of the computed DOS is usually tested by calculating the absorption coefficient, as it is almost proportional to the  $4p$  DOS. This is shown in Fig. 4, where the experimental Cu *K*-edge spectrum of  $\text{KCuF}_3$  is compared with the absorption coefficient obtained from the calculated  $4p$  DOS of Cu by Takahashi *et al.* (2003) and Bingelli & Altarelli (2004). This procedure is consistent provided that the Cu *K*-edge XANES corresponds to a single-channel excitation. However, if the XANES spectrum was due to the superposition of different absorption channels, as found before for Cu–N (Chaboy *et al.*, 2005) and in this study for Cu–O systems, it would lead to unreliable results.

With the aim of determining whether the Cu *K*-edge XANES spectrum of  $\text{KCuF}_3$  is due to a single or double excitation process we have extended our investigation to the  $\text{KCuF}_3$  case. The crystal structure of  $\text{KCuF}_3$  is made up of an array of  $\text{CuF}_6$  octahedra, the distance between  $\text{Cu}^{2+}$  ions being almost the same along the three principal axes. Each  $\text{CuF}_6$  octahedron is slightly elongated along the *a* and *b* axes such that the distortion is orthogonal to that of the neighboring


**Figure 4**

Comparison of the experimental Cu *K*-edge spectrum of  $\text{KCuF}_3$  (circles), adapted from Paolasini *et al.* (2002), and the absorption coefficient obtained from the calculated  $4p$  density of states of Cu by Takahashi *et al.* (2003) (solid line) and by Bingelli & Altarelli (2004) (dotted line).

octahedra in the plane. The structure contains two distinct fluorine ions: (i)  $F_1$  (bond centered) ions located between the *ab* planes and occupying symmetric positions, and (ii)  $F_2$  ions in the *ab* planes. The  $F_2$  ions are slightly displaced, in the opposite (type *a*) or same (type *d*) directions, from the midpoint of adjacent Cu sites (Hidaka *et al.*, 1998). The distorted  $\text{CuF}_6$  octahedron contains two  $F_1$  ions at 1.96 Å from Cu and two pairs of  $F_2$  ions with interatomic Cu– $F_2$  distances  $R = 1.88$  Å and 2.26 Å, respectively. The Cu *K*-edge XANES of  $\text{KCuF}_3$  is shown in Fig. 5. It is characterized by (i) a shoulder (A) at the threshold; (ii) an asymmetric absorption line showing a main peak ( $B_1$ ) at ~7 eV above the edge and a second shoulder ( $B_2$ ) at the high-energy side (~12.5 eV); (iii) a positive peak (C) at ~21 eV above the edge and, finally, (iv) three well defined spectral features, D (~37 eV), E (~52 eV) and F (~72 eV), at high energy. The width of the main absorption line is comparable with that of the previously studied Cu(II) compounds (see Fig. 2), suggesting also the presence of different excitation channels. We have initially calculated the Cu *K*-edge absorption within a single-channel frame by using both non-SCF  $X_\alpha$  and Hedin–Lundqvist potentials for different cluster sizes. The smallest cluster was built by including the first *F* and *K* coordination shells around absorbing Cu ( $R_{\text{max}} = 3.5$  Å) (Hidaka *et al.*, 1998). The calculation performed for this cluster, shown in Fig. 5(a), reproduces the peak at the edge and the high-energy features (D to F). However, only a single main peak without trace of both shoulder  $B_2$  and peak C is obtained. Addition of further shells, including atoms located within a maximum interatomic distance of 4.7 Å around copper, reproduces the  $B_2$  peak. Similar results are found by extending the maximum interatomic distance to 5.9 Å and 7.1 Å around copper (see Fig. 5a). However, the calculations fail in reproducing the intensity ratio of both  $B_1$  and  $B_2$  features and in reproducing peak C. The latter result strongly suggests that the omission of peak C in the calculations is not due to a structural effect. Conse-

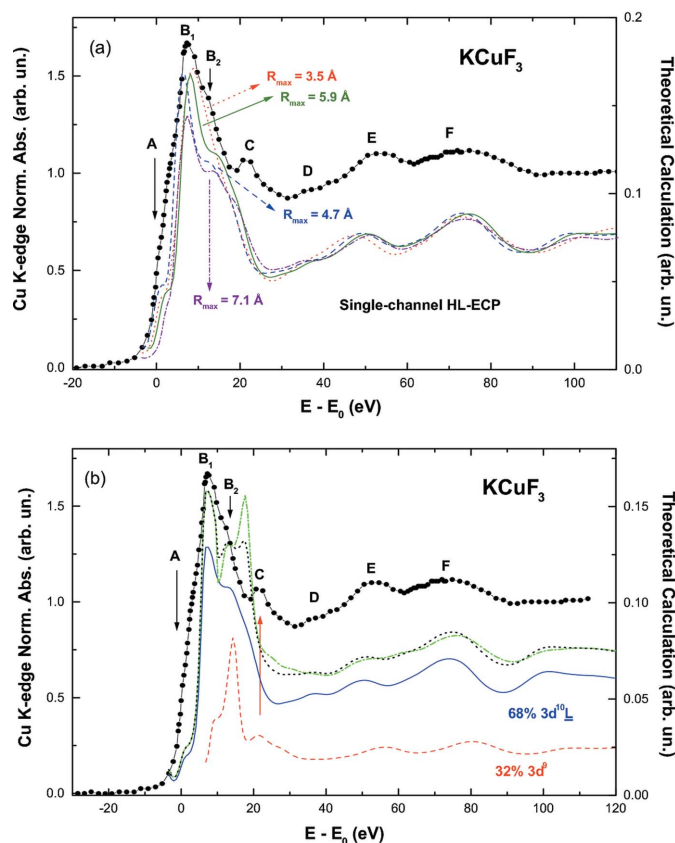


**Figure 5**

(a) Comparison of the experimental Cu  $K$ -edge spectrum of  $\text{KCuF}_3$  (circles) and the spectra calculated by using a complex Hedin–Lundqvist ECP and different clusters with a maximum distance around Cu of  $R_{\text{max}} = 3.5$  Å (dotted line), 4.7 Å (dashed line), 5.9 Å (solid line) and 7.1 Å (dot-dashed line). (b) Comparison of the experimental spectrum and the theoretical calculations obtained for both  $3d^9$  (dashed line) and  $3d^{10}\underline{L}$  (solid line) after applying a 32% and 68% weighting factor. The weighted sum obtained according to the 68:32 (dot-dashed line) and 84:16 (dotted line) ratios is shown (see text for details).

quently, we have studied whether the presence of a second absorption channel can account for the missed structure. Then, we stabilized a SCF potential for a regular  $[\text{CuF}_6]^{4-}$  cluster with an averaged Cu–F distance of  $R = 1.96$  Å. The whole cluster was neutralized by using an outer sphere with a 4+ charge embedded in the larger (*i.e.* distorted) ones to perform the multiple-scattering calculations. In this case the SCF potential was stabilized for both  $3d^9$  and  $3d^{10}\underline{L}$  electronic configurations, where  $\underline{L}$  denotes a hole in F from the ligand. This procedure gives rise to two absorption edges shifted in energy by  $\Delta = 10.3$  eV. According to this calculation, reported in Fig. 5(b), the main peak B<sub>1</sub> is due to the  $3d^{10}\underline{L}$  channel, while both the B<sub>2</sub> shoulder and feature C result from the competition of both  $3d^{10}\underline{L}$  and  $3d^9$  channels. These results suggest the existence of two competitive ionization channels for the  $K$ -edge of divalent copper also in the  $\text{KCuF}_3$  system. Finally, a special comment is deserved for the relative weighting factor for the two absorption channels. Using both 68:32 and 84:16 weighting ratios led to the appearance of an additional peak close to the B<sub>2</sub> shoulder, resembling the C peak previously missing in the calculations. However, the

comparison between the experimental and calculated intensity ratio of both B<sub>1</sub> and B<sub>2</sub> features is not so straightforward. Moreover, the reproduction of the high-energy features (D to F) worsens by using the two-channels computation as compared with the single-channel ones, especially regarding feature E. In the absence of an appropriate multichannel multiple-scattering code (Natoli *et al.*, 1990; Krüger & Natoli, 2004), these results can be related to both interchannel interference (Wu *et al.*, 1996) and to the presence of additional channels, as well as to the need to perform the SCF calculation for a larger distorted octahedron including further cations beyond the first Cu–F coordination shell. Indeed, while in both Cu–N and Cu–O cases the nearest neighborhood of Cu is formed for four ligands in a regular square-planar geometry, it is strongly distorted in the case of  $\text{KCuF}_3$  because of the presence of both bond-centered and displaced F<sub>2</sub> and F<sub>1</sub> ions.

#### 4. Summary and conclusions

We have thoroughly analyzed the Cu  $K$ -edge XANES spectra of the Cu(II) compounds CuO and  $\text{KCuF}_3$ . Detailed theoretical computations of the Cu  $K$ -edge spectra have been performed within the multichannel multiple-scattering framework.

The comparison between the experimental data and computations indicates that the experimental spectra can be accounted for by using two electronic configurations ( $3d^9$  and  $3d^{10}\underline{L}$ ,  $\underline{L}$  being a hole from a ligand) within the sudden limit of the multichannel multiple-scattering theory. Moreover, the use of self-consistency field potentials for the photoabsorbing Cu and its next-neighboring atoms provides a more realistic charge density than that obtained by using the standard neutral atom approximation.

These results are in agreement with previous findings obtained for  $\text{NdCuO}_4$  (Wu *et al.*, 1996), the hydrated  $\text{Cu}^{2+}$  complex in aqueous solution (Chaboy *et al.*, 2006) and Cu–N systems (Chaboy *et al.*, 2005) suggesting that the two-channels ( $3d^9$  and  $3d^{10}\underline{L}$ ) scheme is the general case for the  $K$ -edge XANES of divalent copper systems. This result appears to be independent of both the local environment around Cu as well as of the nature of the ligand. In addition, it is shown that the energy shift between both absorption channels is sensitive to the nature of the bonded atom (N, O, F). By contrast, the relative weight of both  $3d^{10}\underline{L}$  and  $3d^9$  channels is close to the 70:30 ratio in all the studied cases with the exception of  $\text{KCuF}_3$ , for which the agreement between the two-channels computation and the experimental spectrum is not so straightforward. These results, which could stimulate further theoretical work beyond single-configuration approximations, provide a way to face the study of complex Cu systems, including copper oxides or living organisms, by means of XANES.

This work was partially supported by the Spanish CICYT MAT2005-06806-C04-04 and CTQ2005-03657 grants. We wish also to acknowledge F. Carrera and P. Merklings for many friendly and fruitful discussions. ESRF is acknowledged for

beam-time allocation at the BM29 line (experiment number CH-1192).

## References

- Ankudinov, A., Ravel, B., Rehr, J. & Conradson, S. (1998). *Phys. Rev. B*, **58**, 7565–7576.
- Ascone, I., Meyer-Klaucke, W. & Murphy, L. (2003). *J. Synchrotron Rad.* **10**, 16–22.
- Benfatto, M., Natoli, C. R., Bianconi, A., García, J., Marcelli, A., Fanfoni, M. & Davoli, I. (1986). *Phys. Rev. B*, **34**, 5774–5778.
- Benfatto, M., Solera, J. A., Chaboy, J., Proietti, M. G. & García, J. (1997). *Phys. Rev. B*, **56**, 2447–2452.
- Bingelli, N. & Altarelli, M. (2004). *Phys. Rev. B*, **70**, 085117.
- Bocharov, S., Kirchner, T., Dräger, G., Siper, O. & Simnek, A. (2001). *Phys. Rev. B*, **63**, 045104.
- Briois, V., Lagarde, P., Brouder, C., Saintavit, P. & Verdager, M. (1995). *Physica B*, **208–209**, 51–52.
- Carrera, F., Sánchez Marcos, E., Merklings, P. J., Chaboy, J. J. & Muñoz-Páez, A. (2004). *Inorg. Chem.* **43**, 6674–6683.
- Chaboy, J., Muñoz-Páez, A., Carrera, F., Merklings, P. & Sánchez Marcos, E. (2005). *Phys. Rev. B*, **71**, 134208.
- Chaboy, J., Muñoz-Páez, A., Merklings, P. J. & Sánchez Marcos, E. (2006). *J. Chem. Phys.* **124**, 064509.
- Clementi, E. & Roetti, C. (1974). *Atom. Data Nucl. Data Tables*, **14**, 177–478.
- D'Angelo, P., Benfatto, M., Longa, S. D. & Pavel, N. V. (2002). *Phys. Rev. B*, **66**, 064209.
- Hidaka, M., Eguchi, T. & Yamada, I. (1998). *J. Phys. Soc. Jpn.* **67**, 2488–2494.
- Iwasawa, Y. (1996). Editor. *X-ray Absorption Fine Structure for Catalysts and Surfaces*. Singapore: World Scientific.
- Joly, Y. (2001). *Phys. Rev. B*, **63**, 125120.
- Krause, M. O. & Oliver, J. H. (1979). *J. Phys. Chem. Ref. Data*, **8**, 329–338.
- Krüger, P. & Natoli, C. (2004). *Phys. Rev. B*, **70**, 245120.
- Lee, P. A. & Beni, G. (1977). *Phys. Rev. B*, **15**, 2862–2883.
- Mattheis, L. (1964). *Phys. Rev. A*, **133**, 1399–1403.
- Merklings, P. J., Muñoz-Páez, A. & Sánchez Marcos, E. (2002). *J. Am. Chem. Soc.* **124**, 10911–10920.
- Merklings, P. J., Muñoz-Páez, A., Pappalardo, R. R. & Sánchez Marcos, E. (2001). *Phys. Rev. B*, **64**, 092201.
- Nadai, C. D., Demourgues, A. & Grannec, J. (1997). *Nucl. Instrum. Methods Phys. Res. B*, **133**, 1–7.
- Natoli, C. R. & Benfatto, M. (1986). *J. Phys. (Paris) Colloq.* **47**, C8–11.
- Natoli, C. R., Benfatto, M., Brouder, C., Lopez, M. F. R. & Foulis, D. L. (1990). *Phys. Rev. B*, **42**, 1944–1968.
- Natoli, C. R., Benfatto, M., Della Longa, S. & Hatada, K. (2003). *J. Synchrotron Rad.* **10**, 26–42.
- Norman, J. (1974). *Mol. Phys.* **81**, 1191–1198.
- Paolasini, L., Caciuffo, R., Sollier, A., Ghigna, P. & Altarelli, M. (2002). *Phys. Rev. Lett.* **88**, 106403.
- Pedio, M., Benfatto, M., Aminpirooz, S. & Haase, J. (1994). *Phys. Rev. B*, **50**, 6596–6602.
- Sayers, D. E. & Bunker, B. A. (1988). In *X-ray Absorption: Principles, Applications, Techniques of EXAFS, SEXAFS, and XANES*, edited by D. C. Koningsberger and R. Prins, ch. 6. New York: Wiley.
- Siper, O. (1992). *J. Phys. Condens. Matter*, **4**, 9389–9400.
- Takahashi, M., Usuda, M. & Igarashi, J. (2003). *Phys. Rev. B*, **67**, 064425.
- Wu, Z., Benfatto, M. & Natoli, C. (1992). *Phys. Rev. B*, **45**, 531–534.
- Wu, Z., Benfatto, M. & Natoli, C. (1996). *Phys. Rev. B*, **54**, 13409–13412.